



HAL
open science

The E3 ubiquitin ligase TRIP12 is required for pancreatic acinar cell plasticity and pancreatic carcinogenesis

Manon Brunet, Claire Vargas, Marjorie Fanjul, Damien Varry, Naïma Hanoun, Dorian Larrieu, Laetitia Pieruccioni, Guillaume Labrousse, Hubert Lulka, Florence Capilla, et al.

► **To cite this version:**

Manon Brunet, Claire Vargas, Marjorie Fanjul, Damien Varry, Naïma Hanoun, et al.. The E3 ubiquitin ligase TRIP12 is required for pancreatic acinar cell plasticity and pancreatic carcinogenesis. *Journal of Pathology*, 2024, 263 (4-5), pp.466-481. 10.1002/path.6298 . hal-04819617

HAL Id: hal-04819617


<https://hal.science/hal-04819617v1>

Submitted on 4 Dec 2024

HAL is a multi-disciplinary open access archive for the deposit and dissemination of scientific research documents, whether they are published or not. The documents may come from teaching and research institutions in France or abroad, or from public or private research centers.

L'archive ouverte pluridisciplinaire **HAL**, est destinée au dépôt et à la diffusion de documents scientifiques de niveau recherche, publiés ou non, émanant des établissements d'enseignement et de recherche français ou étrangers, des laboratoires publics ou privés.

The E3 ubiquitin ligase TRIP12 is required for pancreatic acinar cell plasticity and pancreatic carcinogenesis

Manon Brunet^{1,2}, Claire Vargas¹, Marjorie Fanjul¹, Damien Varry¹, Naïma Hanoun¹, Dorian Larrieu¹, Laetitia Pieruccioni³, Guillaume Labrousse¹, Hubert Lulka¹, Florence Capilla⁴, Alban Ricard¹, Janick Selves⁵, Anne Couvelard⁶, Véronique Gigoux¹, Pierre Cordelier¹, Julie Guillemet-Guibert¹, Marlène Dufresne^{1†} and Jérôme Torrisani^{1*†} 

¹ CRCT, Université de Toulouse, INSERM, CNRS, Université Toulouse III-Paul Sabatier, Centre de Recherches en Cancérologie de Toulouse, Toulouse, France

² Institut National de la Santé et de la Recherche Médicale (INSERM), UI 297, Institut des Maladies Métaboliques et Cardiovasculaires, Toulouse, France

³ Centre de recherches RESTORE, Université de Toulouse, INSERM, CNRS, EFS, ENVT, Toulouse, France

⁴ Service d'Histopathologie expérimentale, INSERM US006-CREFRE, Toulouse, France

⁵ Département de Pathologie, Institut Universitaire du Cancer Toulouse Oncopole, Toulouse, France

⁶ Département de Pathologie Beaujon-Bichat, Hôpital Bichat, APHP and Université Paris Cité, Paris, France

*Correspondence to: J Torrisani, CRCT, 2 Avenue Hubert Curien, 31 037 Toulouse, France. E-mail: jerome.torrisani@inserm.fr

†These authors contributed equally to this work.

Abstract

The E3 ubiquitin ligase thyroid hormone receptor interacting protein 12 (TRIP12) has been implicated in pancreatic adenocarcinoma (PDAC) through its role in mediating the degradation of pancreas transcription factor 1a (PTF1a). PTF1a is a transcription factor essential for the acinar differentiation state that is notably diminished during the early steps of pancreatic carcinogenesis. Despite these findings, the direct involvement of TRIP12 in the onset of pancreatic cancer has yet to be established. In this study, we demonstrated that TRIP12 protein was significantly upregulated in human pancreatic preneoplastic lesions. Furthermore, we observed that TRIP12 overexpression varied within PDAC samples and PDAC-derived cell lines. We further demonstrated that TRIP12 was required for PDAC-derived cell growth and for the expression of E2F-targeted genes. Acinar-to-ductal cell metaplasia (ADM) is a reversible process that reflects the high plasticity of acinar cells. ADM becomes irreversible in the presence of oncogenic *Kras* mutations and leads to the formation of preneoplastic lesions. Using two genetically modified mouse models, we showed that a loss of TRIP12 prevented acini from developing ADM in response to pancreatic injury. With two additional mouse models, we further discovered that a depletion of TRIP12 prevented the formation of *Kras*^{G12D}-induced preneoplastic lesions and impaired metastasis formation in the presence of mutated *Kras*^{G12D} and *Trp53*^{R172H} genes. In summary our study identified an overexpression of TRIP12 from the early stages of pancreatic carcinogenesis and proposed this E3 ubiquitin ligase as a novel regulator of acinar plasticity with an important dual role in initiation and metastatic steps of PDAC.

© 2024 The Authors. *The Journal of Pathology* published by John Wiley & Sons Ltd on behalf of The Pathological Society of Great Britain and Ireland.

Keywords: thyroid hormone receptor interacting protein 12; pancreatic cancer; preneoplastic lesions; acinar-to-ductal metaplasia; TRIP12; E3 ubiquitin ligase

Received 14 November 2023; Revised 15 March 2024; Accepted 23 April 2024

No conflicts of interest were declared.

Introduction

Pancreatic adenocarcinoma (PDAC), or pancreatic cancer, is the fourth leading cause of death by cancer in Western countries with a 5-year survival rate below 10% [1] that is attributed to the lack of early diagnostic markers and effective treatments. Currently, surgery and a limited number of therapeutic options are available to patients [gemcitabine, folfirinnox, Nab-paclitaxel, or poly-ADP

ribose polymerase (PARP) inhibitors] [2,3]; however, those treatments continue in most cases to be ineffective against PDAC. Thus, gaining a deeper understanding of the mechanisms governing the initiation and progression of PDAC remains crucial. Numerous studies have highlighted not only the remarkable plasticity of acinar cells as a defensive response to prolonged stress [4–8] but also the plasticity of every pancreatic cell type in the setting of neoplastic transformation [9–14]. These

studies have demonstrated that PDAC can arise from ductal and nonductal cells. Moreover, it is known that acinar cells lose their identity upon inflammation or *in vitro* culture via acinar-to-ductal metaplasia (ADM) [15–17]. They dedifferentiate to an intermediate embryonic state and subsequently transdifferentiate to a ductal phenotype [5,18]. Changes in acinar identity increase the malignant transformation of pancreatic cells [19–23]. It is accepted that acinar cells contribute to the development of preneoplastic pancreatic intraepithelial neoplasms (PanIN). Moreover, preventing or reversing tumor initiation in mice may be achieved by maintaining or reintroducing pancreas transcription factor 1A (PTF1A), a key regulator of acinar cell differentiation [24,25], in the presence of *Kras*^{G12D} and inflammation [26–28]. Therefore, preserving a stable acinar cell differentiation program acts as a protective barrier against PDAC [29–31].

Among the proteins involved in the ubiquitin-mediated degradation pathway, the protein thyroid hormone receptor interacting protein 12 (TRIP12) belongs to the homologous E6-AP carboxyl terminus (HECT) E3 ubiquitin ligase family. It participates in the control of major biological processes such as cell proliferation, chromatin remodeling, and DNA damage repair [32–38]. TRIP12 expression is correlated with the prognosis of hepatocellular carcinoma [39] and affects the radiosensitivity of human papilloma virus-positive head and neck squamous carcinoma [40]. It also constitutes a potential marker of response to PARP inhibitors in BRCAness patients [37]. We showed that TRIP12 expression was tightly regulated during the cell cycle, which is important for mitosis and chromosome stability [41]. Studies indicate that TRIP12 regulates the stability of critical proteins involved in determining the cellular origins of PDAC. For example, TRIP12 targets the degradation of F-box and WD repeat domain containing 7 (FBW7), a major regulator of pancreatic ductal cell fate and a tumor suppressor in a subset of PDAC patients [42]. We previously showed that TRIP12 ubiquitinated PTF1A and induced its degradation by the proteasome [43]. Yet the expression level of TRIP12 and its role in pancreatic carcinogenesis have not been thoroughly explored.

In this study, we examined the expression of the TRIP12 protein in human preneoplastic lesions and tumor samples. Employing various transgenic mouse models, we assessed the impact of TRIP12 on acinar cell plasticity and the development of pancreatic cancer.

Materials and methods

Clinical samples

Surgically resected PDAC specimens from 27 patients and a human PDAC tissue microarray were obtained from the Department of Pathology of the Cancer University Institute of Toulouse (Toulouse, France) following approval by the ethics committee of Toulouse Hospital. Patients' samples were obtained after informed

consent was obtained and in accordance with the Declaration of Helsinki. Human tissue samples containing intraductal papillary mucinous neoplasms (IPMN) were provided by the Department of Pathology of Beaujon Hospital (Clichy, France). Seventy-seven paraffin-embedded IPMN lesions were included in a tissue microarray. Samples were immunostained with anti-TRIP12 antibodies (supplementary material, Table S1) using standard procedures. The intensity of TRIP12 nuclear staining in PDAC tissue microarray was graded as weak, moderate, and strong by four independent observers (MB, JS, MD, and JT).

Mouse models, treatments, and orthotopic grafts

To generate conditional *Trip12* knockout mice, embryonic stem (ES) cell clones carrying the targeted allele (*Trip12*^{tm1a(KOMP)Wtsi}) were obtained from the Knockout Mouse Project repository (University of California, Davis, CA, USA. mmrc@ucdavis.edu). Targeted ES cell clones were microinjected into blastocysts of C57BL/6 mice to generate the Tm1a line, which was crossed with a Flpo-recombinase deleter strain (European Mouse Mutant Archive repository, Neuherberg/Munich, Germany) to generate *Trip12*^{tm1c} *Ciphe* mice carrying the floxed allele. All animal studies were approved by the Ministère de l'Éducation Nationale, de l'Enseignement Supérieur et de la Recherche (APAFIS#3600-201512160838611v3) and performed in accordance with institutional guidelines. The following strains were previously described: the *LSL-Kras*^{G12D} and *LSL-Trp53*^{R172H} knock-in mice were obtained from the Mouse Models of Human Cancers Consortium repository (NCI-Frederick, MD, USA), and *Pdx1-Cre* mice were obtained from Dr. D.A. Melton (Harvard University, Cambridge, MA, USA). Elastase Cre^{ERT2} mice (*Elas-CreERT2*) were generated by Dr. D.A. Stoffers (Philadelphia, PA, USA) [44] and were provided by Dr. P. Jacquemin (UCL, Belgium, Brussels). ZsGreen mice (B6.Cg-Gt(ROSA)26Sor^{tm6(CAG-ZsGreen1)Hze/J}) were obtained from the Jackson Laboratory (Bar Harbor, ME, USA). Mice were interbred on a mixed background to obtain *Pdx1-Cre;Trip12*^{fl/fl} (CT mice), *Elas-CreERT2;Trip12*^{fl/fl} (ET mice), *LSL-Kras*^{G12D};*Trip12*^{fl/fl};*Elas-CreERT2* (KET mice), and *LSL-Kras*^{G12D};*LSL-Trp53*^{R172H};*Trip12*^{fl/fl};*Pdx1-Cre* (KPCT mice).

Seven-week-old ET and control (E) mice were treated with tamoxifen (20 mg/ml; Sigma-Aldrich, St. Louis, MO, USA) dissolved in corn oil with 10% ethanol. Mice received three intraperitoneal (i.p.) injections (1 mg/15 g body weight) on three consecutive days. Acute pancreatitis was induced at 8 weeks by two sets of 6-hourly i.p. injections of caerulein (50 µg/kg; Sigma-Aldrich) on alternating days. Mice were sacrificed after 2, 24, and 120 h and 7 weeks. Blood and tissue samples were collected. Amylase concentration was measured in plasma using alpha-amylase assay (Phadebas, Kristantad, Sweden). Glycemia was determined using a glucose monitoring kit (Accu-Chek Performa, Roche, Meylan, France). Glucose (2 g/kg, Sigma-Aldrich) was

injected i.p., and glycemia was measured at the indicated times.

Gaussia Luciferase MIA PaCa-2 shScr and shTRIP12#1 (2×10^6 cells/injection) were injected into the pancreas of severe combined immunodeficiency mice. Luciferase activity was determined after injection of coelenterazine (Promega, Madison, WI, USA) every 4–5 days after injection as described previously [45].

Acinar cell isolation and *ex vivo* ADM formation

Pancreata were resected, and 100 mg of each was placed in cold Hank's balanced salt solution (Gibco/BRL, Gaithersburg, MD, USA) containing 0.01% soybean trypsin inhibitor (STI) (Sigma-Aldrich) and 1,000 U of collagenase II (Thermo Fisher Scientific, Carlsbad, CA, USA). Digestion was performed at 37 °C for 20 min with mechanical dissociation. Digested pancreatic tissue was pelleted, centrifuged, and suspended in DMEM culture medium containing 4.5 g/l glucose, 10% fetal bovine serum (FBS, Eurobio Scientific, Les Ulis, France), 10% penicillin–streptomycin mixture, and 0.01% STI. Epidermal growth factor (EGF, 20 ng/ml; Sigma-Aldrich) was added to the acinar cell suspension. An equal volume of rat tail collagen (RTC)-type I (Corning, Corning, NY, USA) was added, and 500 μ l were seeded on precoated 24-well dishes with 100 μ l of RTC then incubated at 37 °C in 5% CO₂. After RTC solidification, complete DMEM culture medium (Gibco/BRL) was added and changed at days 1 and 4. ADM was quantified using a Z1 microscope (Zeiss, Baden-Württemberg, Germany) and Fiji software (<https://imagej.net/software/fiji/downloads>).

Generation of mouse cancer cell lines and tail vein injections

Pancreatic tumors from KPC and KPCT mice were cut into $\sim 1\text{-mm}^3$ pieces and transferred to DMEM-F12 (Gibco/BRL) culture medium (with 10% FBS and antibiotics). The medium was renewed every 3 days. Primary cultures were monitored for 15–35 days for epithelial cell outgrowth. The primary outgrowing epithelial cells were subcultured by trypsinization using a 0.05% trypsin–0.02% EDTA solution (Thermo Fisher Scientific). From the second passage, the cells were maintained in DMEM-F12 medium containing 10% FBS and antibiotics. Mouse pancreatic cancer cells (1×10^6) were injected into the tail vein of 8-week-old C57/B6 mice. Four weeks after injection, lungs were inflated with formalin then embedded in paraffin wax.

Histological analysis, immunohistochemistry, and immunofluorescence

Pancreata were fixed in 10% neutral buffered formalin and embedded in paraffin wax. For histopathological analysis, pancreata were serially sectioned at 4 μ m and stained with hematoxylin and eosin (H/E). Histopathological analysis and scoring of tissue damage

were performed using representative serial H/E-stained sections. Immunostaining followed standard protocols. Antibodies used for immunohistochemical analyses are listed in supplementary material, Table S1. Sections were imaged using a Hamamatsu Nanozoomer 2 slide scanner (Hamamatsu Photonics, Shizuoka, Japan) or a Panoramic 250 flash II Scanner (3DHISTECH, Budapest, Hungary). Images were analyzed and quantified using CaseViewer (3DHISTECH) or QuPath 5.0 software [46].

Statistical analysis

The GraphPad Prism 9 software package (GraphPad Software, Boston, MA, USA) was used to perform statistical tests as mentioned in the figure legends. A difference was considered significant when the *p* value was less than 0.05. The number of independent experiments is indicated in the figure legends. *, **, ***, and **** indicate a *p* value <0.05, 0.01, 0.001, and 0.0001, respectively.

Details for disease-free survival analysis, cell lines and culture, comparative genomic hybridization array, sodium bisulfite mapping, cell adhesion tests, cell cycle synchronization, immunofluorescence on PDAC-derived cell lines, shRNA lentiviral plasmids and lentiviral production, flow cytometry, RNA isolation and semi-quantitative real-time polymerase chain reaction (PCR) analysis, western blot analysis, Agilent microarray gene expression analysis, protein–protein interaction network analysis, RNA sequence analysis, Gene Set Enrichment Analysis (GSEA), and cell growth rate, colony formation, and invasion assays are presented in Supplementary materials and methods.

Results

TRIP12 is overexpressed in human preneoplastic lesions and pancreatic tumors

The TRIP12 protein was observed in the nuclei of exocrine acinar and ductal cells, as well as in the endocrine islets of healthy pancreas tissue, although the staining intensity was notably weak and exhibited heterogeneity (Figure 1A). A significant increase in TRIP12 staining intensity was measured in pancreatic intra-epithelial neoplasia (PanIN) (Figure 1B,C) and in IPMN lesions (Figure 1D,E). We also found that TRIP12 was markedly overexpressed in PDAC samples (Figure 1C–F), which was supported by *TRIP12* mRNA expression in public datasets (Figure 1G). Moreover, a tissue microarray revealed a great heterogeneity of TRIP12 expression in PDAC that was not correlated with gender, age, grade, or differentiation state (Figure 1H and supplementary material, Table S3). A similar heterogeneity of TRIP12 overexpression was measured in a panel of PDAC-derived cell lines (Figure 1I, and supplementary material, Figure S1A,B). This heterogeneity was not explained by large *Trip12* gene

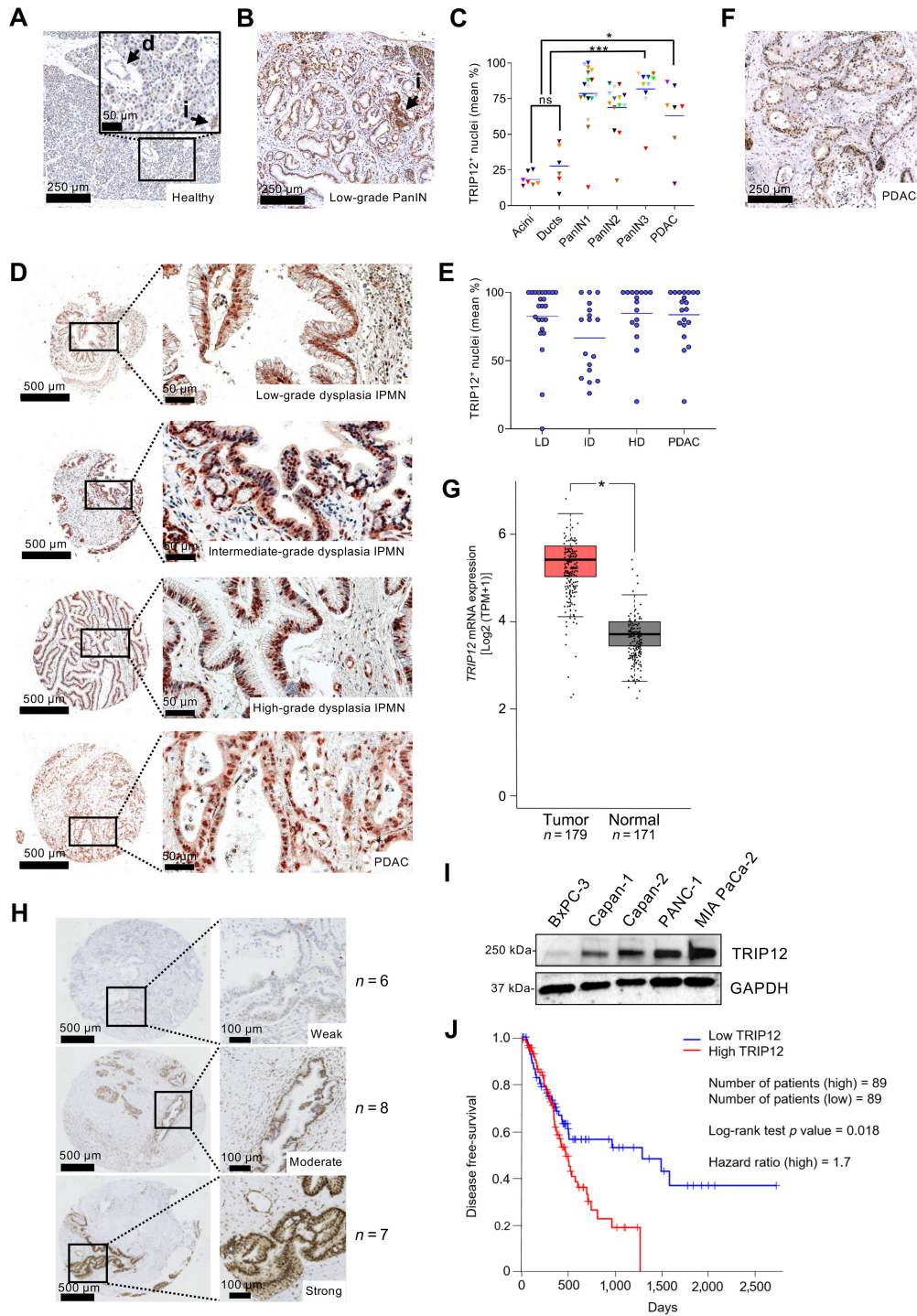


Figure 1. TRIP12 is overexpressed in human preneoplastic lesions and pancreatic tumors. (A) Representative TRIP12 immunohistochemistry (IHC) staining in healthy pancreatic tissue: d, duct; I, islet. (B) Representative TRIP12 IHC staining in sections of human pancreas containing PanINs: I, islet. (C) Quantification of TRIP12-positive nuclei in 29,000 acinar cells from seven PDAC patients, in 85 nonneoplastic ducts from six PDAC patients, in 170 PanIN1, 62 PanIN2, and 29 PanIN3 from 17, 14, and 10 patients, respectively, and in 537 neoplastic ducts from seven PDAC patients. Each symbol represents the mean percentage of TRIP12-positive nuclei in each sample. Each color corresponds to one patient. The blue bars represent the mean of each group. A Mann–Whitney test was used. (D) Representative TRIP12 IHC staining in IPMN with low-grade dysplasia, intermediate-grade dysplasia, and high-grade dysplasia and in PDAC. (E) Percentage of TRIP12-positive nuclei scored in five cores of 27 IPMN with low-grade dysplasia (LD), 17 IPMN with intermediate-grade dysplasia (ID), 20 IPMN with high-grade dysplasia (HD), and in 21 carcinoma (PDAC) cases assessed by two investigators. Blue bars represent the mean of each group. (F) Representative TRIP12 IHC staining in human PDAC. (G) Expression of *TRIP12* mRNA in pancreatic tumors ($n = 179$) and normal pancreas ($n = 171$), obtained from the Gene Expression Profiling Interactive Analysis (GEPIA) public database. A Mantel–Cox test was used. (H) Representative TRIP12 IHC staining obtained on a tissue microarray of human PDAC displaying a weak ($n = 6$), moderate ($n = 8$), and strong ($n = 7$) TRIP12 expression. The insets emphasize cancerous cells. (I) TRIP12 protein expression in five PDAC-derived cell lines determined by western blot analysis. GAPDH protein level was used as loading control. The image is representative of at least three independent experiments. (J) Kaplan–Meier plots of disease-free survival of high (red, $n = 89$) and low (blue, $n = 89$) *TRIP12* mRNA expressing PDAC patients (50th percentile). Data were obtained from the GEPIA database and expressed as survival fraction. A log-rank test was applied.

alterations or promoter hypermethylation (supplementary material, Figure S2A–C). *TRIP12* mRNA variants with short or long 3'-UTR (3'-UnTranslated Region) that display different translation efficiencies were reported [47]. The assessment of *TRIP12* 3'-UTR variants did not reveal significant differences among PDAC-derived cell lines (supplementary material, Figure S3 and Table S2). Nevertheless, we noted a distinct regulation of *TRIP12* during the cell cycle, correlating with its expression in PDAC-derived cell lines (supplementary material, Figure S4A–C). Clinically, high *TRIP12* expression in PDAC is associated with a shorter disease-free survival (Figure 1J).

Collectively, our findings support the role of *TRIP12* overexpression in the initiation and/or progression of PDAC.

TRIP12 participates in human PDAC-derived cell growth and modifies E2F-targeted gene expression

To investigate the implication of *TRIP12* in the fate of human PDAC-derived cells, we generated *TRIP12* depleted-PANC-1 and MIA PaCa-2 cell lines (Figure 2A, supplementary material, Figure S5A,B). The main consequence of *TRIP12* depletion was a significant inhibition of cellular growth *in vitro* (Figure 2B and supplementary material, Figure S5C) but also *in vivo* (Figure 2C and supplementary material, Figure S6A) without affecting cell adhesion (supplementary material, Figure S6B). To better understand how *TRIP12* affects PDAC-derived cell growth, transcriptomic analysis and GSEA were performed. Among the Molecular Signatures DataBase (MSigDB) hallmark gene sets, the most repressed pathway in both *TRIP12*-depleted PDAC-derived cell lines was the E2F-targeted genes (Figure 2D, supplementary material, Table S4 and Figure S7). Among the 195 genes that constitute the E2F target gene set, 90 genes were commonly repressed in both *TRIP12*-depleted cell lines (Figure 2E). E2F transcription factor family controls the transcription of genes involved in G₁-to-S, G₂-to-M transition and DNA damage repair [48]. A functional interaction network of the 195 E2F target gene products illustrated their implication in DNA replication, DNA repair, G₂/M transition of mitotic cycle, and chromosome segregation (supplementary material, Figure S8, top panel). Interestingly, the two latter functional networks were largely conserved in the analysis of E2F target genes repressed in *TRIP12*-depleted MIA PaCa-2 cells (supplementary material, Figure S8, bottom panel). Moreover, the *TRIP12* depletion led to an accumulation of cells in S and G₂ phases suggesting a functional defect in these phases (Figure 2F). Taken together, these findings indicate that *TRIP12* is important for the appropriate growth of PDAC-derived cells. Moreover, they support the involvement of *TRIP12* in regulating the expression of E2F target genes that are crucial for mitotic division.

TRIP12 deficiency during embryogenesis induces pancreatic abnormalities in adults

To investigate the implication of *TRIP12* in the initiation steps of PDAC, we generated conditional *Trip12* knock-out mice by crossing mice carrying floxed alleles of the *Trip12* gene with *Pdx1*-Cre mice to deplete the *TRIP12* protein in embryonic pancreatic progenitors (Figure 3A). *TRIP12*-deficient mice (CT) were viable and indistinguishable in appearance from the control (C) littermates. As expected, the depletion of *TRIP12* was observed in all pancreatic cell types of CT mice pancreas (supplementary material, Figure S9A). While the body weights of CT and C mice were similar at the age of 3 months, we measured a significant alteration of pancreas weight and pancreas to body weight ratio in CT mice that persists in older mice (Figure 3B). Interestingly, H/E staining revealed a pancreatic steatosis in all CT mice pancreases examined at the age of 3–4 months but no other cytological and degenerative changes (Figure 3C).

We conducted i.p. glucose tolerance tests to assess whether the depletion of *TRIP12* in islets influences blood glucose homeostasis. Fasting glycemia was not significantly different in CT mice at the age of 3 months (Figure 3D). However, the response to glucose overload was improved indicating that *Trip12* gene depletion affects pancreatic endocrine function of young adults with no significant difference of islet size (Figure 3E) or insulin and glucagon staining (Figure 3F). We expanded the study of *TRIP12* depletion in acinar cells by a transcriptome analysis. A total of 566 genes were significantly altered (supplementary material, Figure S9B). The analysis of the top 25 most downregulated genes in CT acinar cells underscores the importance of *TRIP12* in maintaining the acinar cell phenotype. Notably, eight of these genes were associated with enzyme production, and seven were involved in the regulation of differentiation (Figure 3G). Gene enrichment analyses revealed changes in genes associated with metabolic and cell morphogenesis, organelles, vacuoles, extracellular matrix, pancreatic secretion, and Notch pathway (supplementary material, Figure S9C). We also identified an effect of *TRIP12* depletion on genes related to acinar cell identity (Figure 3H). Altogether, our results suggest that *TRIP12* deficiency during embryogenesis leads to an altered mature acinar cell identity.

In parallel, we generated an *Elas*-CreERT2 acinar cell-specific conditional disruption of *Trip12* gene by the administration of tamoxifen (supplementary material, Figure S10A). We confirmed an acinar *TRIP12* depletion in ET pancreas (supplementary material, Figure S10B). The pancreas-to-body-weight ratio of *TRIP12*-deficient mice (ET) significantly decreased at 5 months of age. The same trend was observed in older mice (supplementary material, Figure S10C). Unlike *Pdx1*-Cre;*Trip12*^{fl/fl} model, ET mice exhibited no macroscopic modifications of their pancreas, and H/E staining showed similar pancreas phenotypes in E and ET mice (supplementary material, Figure S10D).

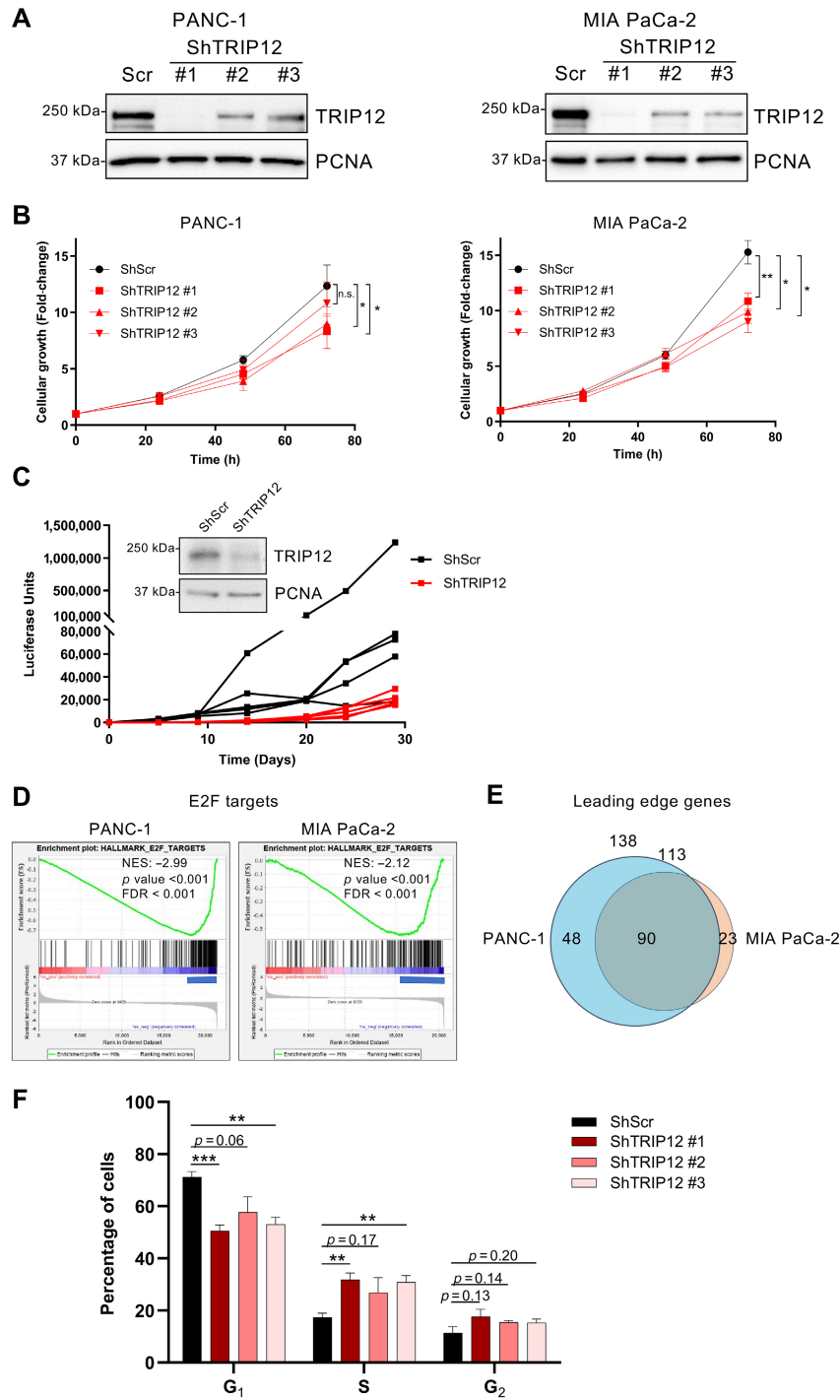


Figure 2. TRIP12 participates in human PDAC-derived cell growth and modifies E2F-targeted gene expression. (A) TRIP12 protein level in PANC-1 and MIA PaCa-2 cells stably expressing three shRNAs directed against *TRIP12* mRNA (ShTRIP12#1, #2, #3) measured by western blotting and compared to its level in PANC-1 and MIA PaCa-2 expressing a control shRNA (ShScr). Proliferating cell nuclear antigen (PCNA) protein level was used as loading control. The image is representative of three independent experiments. Western blot analysis was performed prior to cell growth measurements presented in (B). (B) Cell growth of TRIP12-depleted PANC-1 and MIA PaCa-2 cells determined by seeding at 5×10^5 cells/well and counting every 24 h for 72 h. Mean \pm SEM compared to $t = 0$ h (set as 1). A Mann-Whitney test was used. (C) *In vivo* growth of TRIP12-depleted and control MIA PaCa-2 cells was determined after orthotopic implantation in the pancreas of nude mice. MIA PaCa-2 cells stably expressing *Gaussia* luciferase (GLuc) were stably transfected with ShTRIP12 or Scr shRNA. Luciferase activity in blood was measured every 4–6 days over 29 days. The results show the luciferase activity (LU) across four mice for each condition. The inset represents the level of TRIP12 protein in ShScr and ShTRIP12 GLuc MIA PaCa-2 cells determined by western blotting. PCNA protein level was used as loading control. (D) Graphical representation of E2F target gene set enrichments after TRIP12-depleted PANC-1 and MIA PaCa-2 cell transcriptomic analysis using GSEA software with a nominal p value < 0.001 and a false discovery rate (FDR) < 0.001 . NES, normalized enrichment score. The blue rectangles indicate leading edge genes. (E) Venn diagram representing E2F target leading edge genes in TRIP12-depleted PANC-1 and MIA PaCa-2 cell transcriptomic analysis. (F) Cell-cycle distribution of TRIP12-depleted (ShTRIP12 #1, #2, and #3) and control (ShScr) MIA PaCa-2 cells measured by flow cytometry after propidium iodide incorporation. The results are expressed as percentage of cells in the different phase of the cell cycle and are the mean \pm SEM of at least four independent experiments. An unpaired t -test was used.

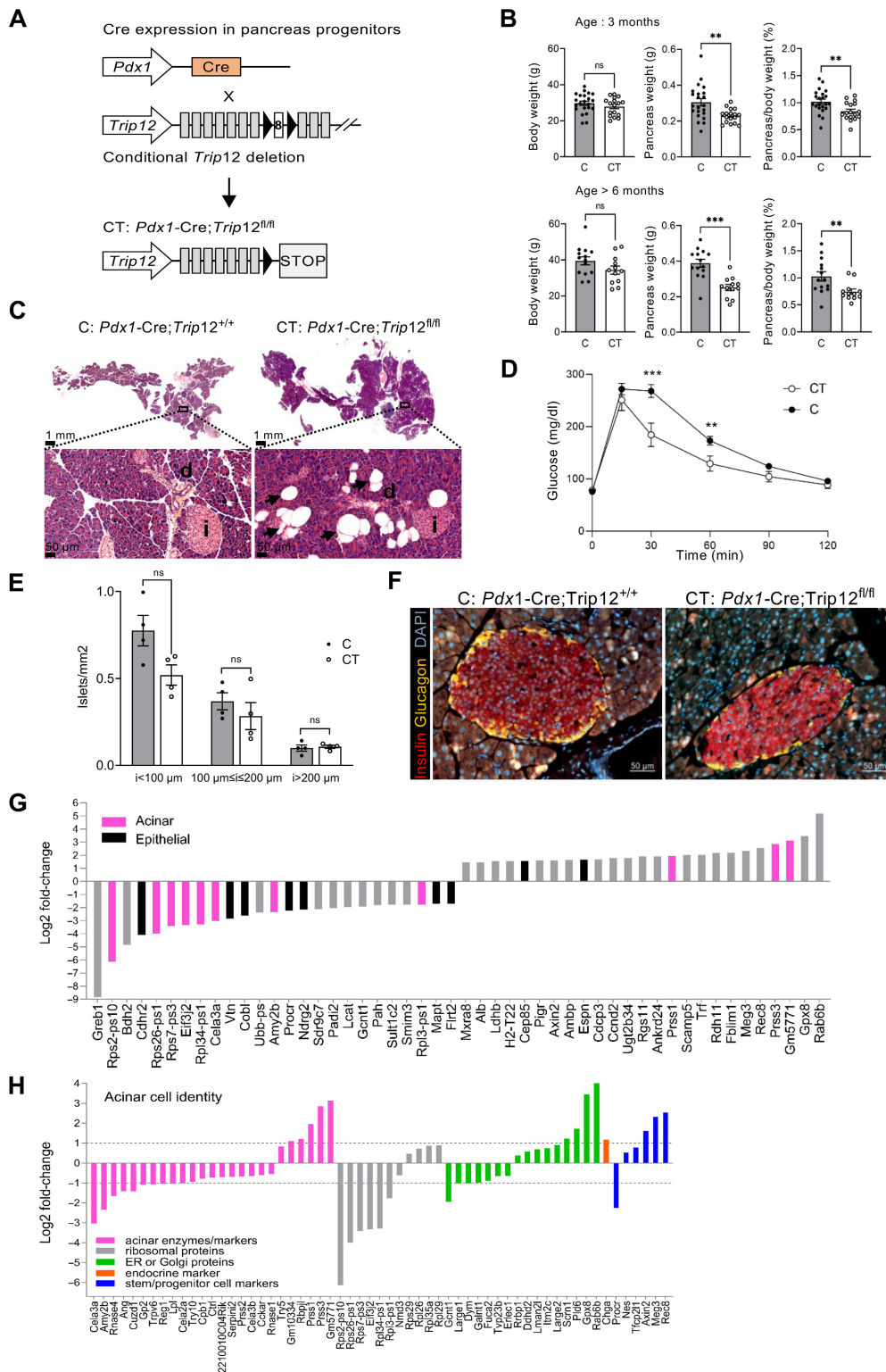


Figure 3. TRIP12 deficiency during embryogenesis induces pancreatic abnormalities in adults. (A) Schematic representation of CT model in which the Cre recombinase expression is driven by the *Pdx1* promoter. Black triangles indicate loxP sequences. (B) Body weight, pancreas weight, and pancreas/body weight ratio of control (C) mice ($n = 22$) and TRIP12-deficient (CT) mice ($n = 17$) at age 3 months and of C ($n = 12$) and CT mice ($n = 14$) older than 6 months. Mean \pm SEM. A Mann–Whitney test was used. (C) Representative hematoxylin/eosin staining of *Pdx1-Cre;Trip12*^{+/+} (C) and *Pdx1-Cre;Trip12*^{fl/fl} (CT) pancreas at age 3 months. Boxes indicate enlarged regions: d, duct; l, islet. Black arrows indicate pancreatic steatosis areas. (D) Glycemia after i.p. glucose injection in C ($n = 21$) and CT ($n = 15$) mice at age 1 to 3 months. A Mann–Whitney test was used. (E) Islets were counted and their diameters measured in two sections of pancreas of C ($n = 4$) and CT ($n = 4$) mice. Mean \pm SEM. A Mann–Whitney test was used. (F) Representative immunofluorescence image of INSULIN (red) and GLUCAGON (yellow) in islets from C and CT mice ($n = 3$). Nuclei were counterstained with DAPI. (G) Graphical representation of 25 most significantly increased or decreased mRNA in CT versus C acinar cells: mRNAs with adjusted p value lower than 0.05 were considered significantly altered. Pink bars represent mRNAs related to acinar cell identity; black bars represent mRNAs related to epithelial phenotype. (H) Graphical representation of acinar cell identity mRNA expression.

TRIP12 is required for ADM formation *ex vivo* and *in vivo*

ADM precedes the formation of PanIN in response to inflammation. Considering the increased expression of TRIP12 observed in early-stage preneoplastic lesions (Figure 1B–E), we explored its role in the regulation of acinar cell plasticity. For these assays we used an established *ex vivo* 3D-acinar cell culture that models the conversion of acinar cells to ductal cells. To this end, CT and ET mice were crossed with ZsGreen Cre reporter mice to generate ZsG-CT and ZsG-ET mice [49] (supplementary material, Figure S11A,B, left panel). As expected, ZsGreen was expressed in acinar, ductal, and islet cells of ZsG-C mice (supplementary material, Figure S11A, right panel) and specifically in acinar cells of ZsG-E mice (supplementary material, Figure S11B, right panel). Acinar cells were isolated from ZsG-CT and ZsG-ET mice and controls (ZsG-C and ZsG-E). Following the addition of EGF, control acini converted to ductal structures after 4 days (Figure 4A,B). In contrast, TRIP12-depleted acinar cells did not transdifferentiate into ductal cells. Interestingly, the ductal structures visible in TRIP12-deficient acinar preparations did not express ZsGreen and corresponded to cells that had failed Cre-mediated recombination (Figure 4A,B, lower panels). The absence of TRIP12 was associated with the presence of abnormal ZsGreen-positive cell clusters corresponding to multilobed structures with lumen or vacuoles devoid of ductal epithelium (Figure 4C,D). These results demonstrate that TRIP12 is required for ADM and contributes to acinar cell plasticity.

We delved deeper into the function of TRIP12 in acinar cell dedifferentiation *in vivo* utilizing a caerulein-induced acute pancreatitis model in E versus ET mice (Figure 4E). The onset of pancreatitis was validated by elevated plasma amylase levels in both groups (Figure 4F). Vacuolization of acinar cells that is indicative of autophagy, stressed acini, or necrosis was noticed in E and ET mice (Figure 4G). In control mice, the initiation of ADM was marked by the distension of acinar lumens, whereas in ET mice, features included acinar hypertrophy, more uniformly distributed eosinophilic zymogen granule zones, and reduced basophilic areas at the base of acinar cells. After 1 day, entire lobules of control mice displayed extensive ADM. In contrast, ET acini retained a hypertrophied acinar phenotype with numerous vacuoles. While the interstitial edema area was similar in both groups, inflammatory cells were less numerous in ET pancreas (supplementary material, Figure S12A,B). After 5 days, most control acinar tissue reverted back to its original morphology, whereas ET acinar tissue retained several defects. Indeed, vacuoles were still present, suggesting that a longer period was required for complete recovery. As expected during ADM, caerulein-treated control mice displayed a peak of cytokeratin 19 (CK19) staining in acinar cells after 1 day that returned to basal level after 5 days (Figure 4H). In ET acini, CK19 expression increased to a lower extent after 1 day, confirming an

altered transdifferentiation. Moreover, CK19 staining was restricted to apical pole around acinar lumen and did not extend in basolateral location as observed in ADM.

Taken together, our experiments demonstrated that TRIP12 was necessary for ADM formation not only *ex vivo* but also *in vivo*. Additionally, its depletion affects the differentiation response to caerulein in the pancreas of mice.

TRIP12 participates in PDAC initiation, metastatic dissemination, and CLAUDIN 18 expression

It is known that *Kras*^{G12D} oncogene expression in adult acinar cells initiates PDAC [50]. We hypothesized that altered ADM observed in the absence of TRIP12 affected PDAC initiation. We generated TRIP12-deficient (KET) and TRIP12-expressing (KE) control mice (Figure 5A). The activation of *Kras*^{G12D} concomitantly with the loss of TRIP12 was obtained by an administration of tamoxifen. Mice were sacrificed 3 months after tamoxifen treatment (Figure 5B). No difference in pancreas/body weight ratio was measured (supplementary material, Figure S13). Histological analyses revealed the presence of low-grade PanINs in four out of seven KE mice but no evidence of PanINs in any of the six KET mice (Figure 5C,D). To confirm these results, KE and KET mice were treated with caerulein a week after tamoxifen treatment (Figure 5E). After 7 weeks, mice were sacrificed and analyzed. As expected, caerulein injections increased the proportion of mice harboring PanIN lesions stained by Alcian blue and (four out of four) displaying an activation of ERK1/2 pathway (Figure 5F,G). In contrast, the absence of preneoplastic lesions in KET was associated with an absence of ERK1/2 pathway activation, confirming that TRIP12 is necessary for the initiation steps of PDAC initiated by oncogenic *Kras*^{G12D}.

Finally, we posited that TRIP12 played a role in the formation and progression of PDAC. To test this hypothesis, we generated mice cohorts of the consensus KPC mouse PDAC model [51] (*Kras*^{G12D} and *Trp53*^{R172H}) expressing TRIP12 (KPC) or not (KPCT) (Figure 6A). Autopsy and histological analyses revealed that both KPC and KPCT mice developed PDAC (Figure 6B,C), indicating that the depletion of TRIP12 was not able to counteract PDAC formation in the combined expression of *Kras*^{G12D} and *Trp53*^{R172H} oncogenes. Nevertheless, KPCT mice displayed a lower tumor incidence (four out of seven versus six out of seven in KPC mice) and less frequent metastasis mainly located on liver and kidneys (Figure 6B). Body and tumor weights of both groups were similar, although the perimeter of KPCT tumors tended to be smaller (supplementary material, Figure S14A,B). The relative surface occupied by tumor cells, pancreatic lesions, and normal acini was not statistically different between the two groups (supplementary material, Figure S14C).

Interestingly, histological analysis revealed that KPC tumors displayed a mesenchymal cellular component that was not observed in KPCT tumors (Figure 6C,D).

The median survival of KPC and KPCT mice was not statistically different but a death delay of KPCT mice was observed (Figure 6E). Subsequently, we generated cell lines from KPC and KPCT tumors (Figure 6F).

Using Boyden chambers, we measured the capacity of KPC and KPCT cells to invade extracellular matrix proteins. Our experiments revealed that the loss of TRIP12 affects the invasive capacity of pancreatic cancer cells

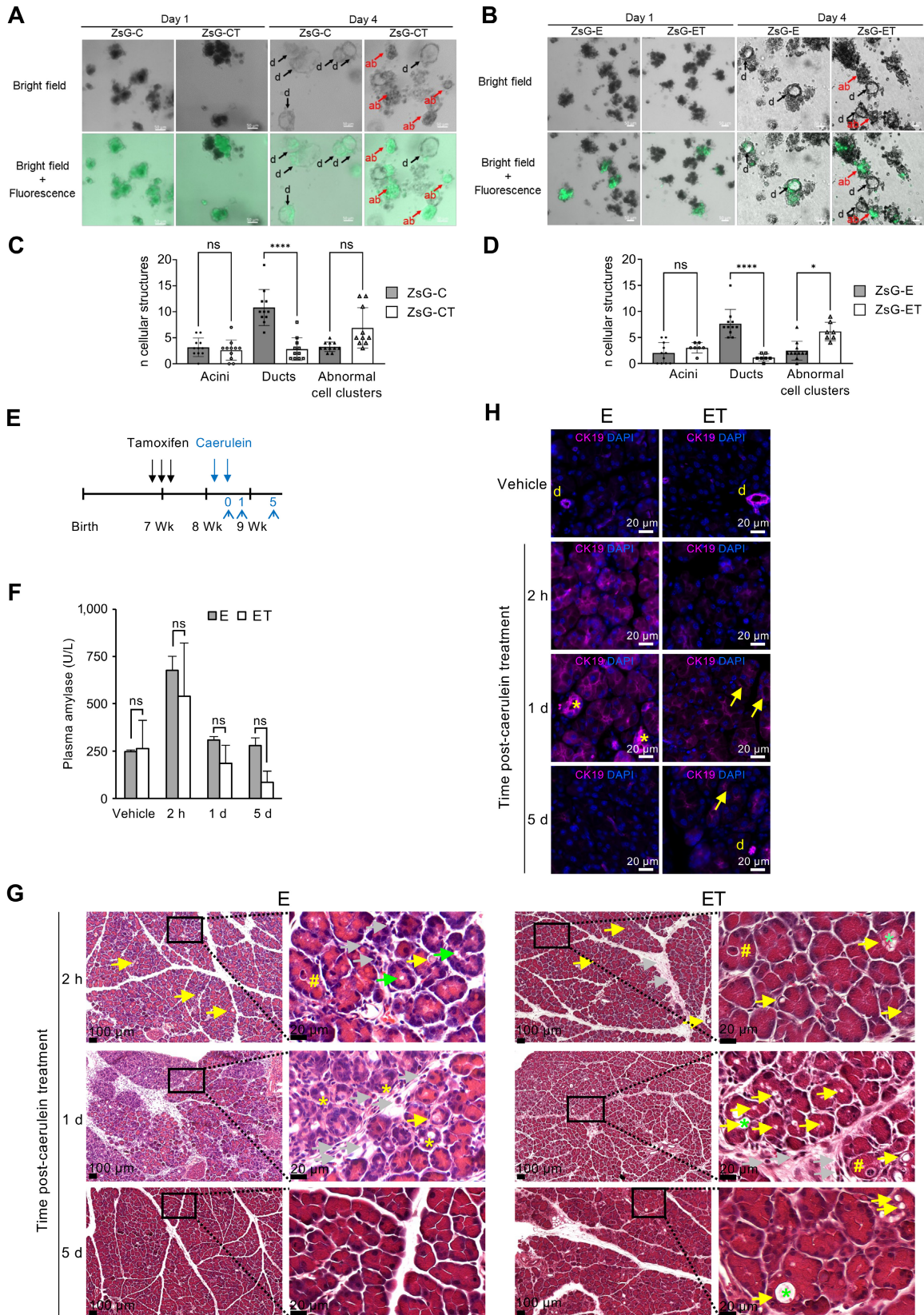


Figure 4 Legend on next page.

(supplementary material, Figure S14D). Moreover, to determine their capacity to form metastasis, KPC and KPCT cells were injected in mice tail vein, a commonly used to model lung metastasis [52]. Injected cells transit through the vena cava and the right heart and reach the lung capillary system. The appearance of metastasis in the lung was measured 4 weeks after injection. This experiment showed that the depletion of TRIP12 inhibits the *in vivo* metastatic dissemination of pancreatic cancer cells (Figure 6G). We further characterized murine tumor-derived cell lines by analyzing their transcriptome. RNA sequencing (RNA-seq) analysis identified 609 altered genes in KPCT cell lines with a dramatic loss of *CLAUDIN18* mRNA expression (Figure 6H). The tight junction CLAUDIN 18 protein is known as an early marker of pancreatic carcinogenesis [53,54]. The specific loss of the gastric *CLAUDIN 18.2* isoform in KPCT cells was demonstrated by RT-qPCR (supplementary material, Figure S14E). Moreover, CLAUDIN 18 loss was confirmed in KPCT-derived cells as well as in KPCT tumors (Figure 6I,J).

Taken together, our findings indicated that TRIP12 was required for PDAC initiation and that it participated in metastatic dissemination. Moreover, they showed that TRIP12 was necessary for the expression of CLAUDIN 18, an early marker of pancreatic carcinogenesis.

Discussion

In this study, we have shown that TRIP12 is expressed at low levels in normal pancreas but is significantly overexpressed in pancreatic preneoplastic lesions and PDAC. Employing two conditional *Trip12* knockout mouse models, we revealed that TRIP12 expression was necessary for the formation of ADM, a critical initial step in the initiation of PDAC. Using two novel murine models, we further showed that TRIP12 deficiency impedes PanIN formation in the presence of *Kras*^{G12D} and reduces the metastatic capacity of tumor cells when *Trp53*^{R172H} is concomitantly expressed.

As mentioned earlier, TRIP12 overexpression in PDAC samples was also observed in other studies [32]. We unveiled a high heterogeneity of TRIP12 expression within PDAC samples that is supported by the human Protein Atlas data. Similarly, TRIP12 heterogeneity was observed in PDAC-derived cell lines that we could not explain by large genomic alterations, DNA hypermethylation, or the level of *Trip12* mRNA 3'-UTR variants [47]. We previously showed that TRIP12 protein expression was tightly regulated during the cell cycle [41]. Herein, we showed that an altered cell cycle regulation of TRIP12 is associated with its expression level and could explain TRIP12 heterogeneous expression in PDAC-derived cells.

We established that TRIP12 was important for the proliferation of human PDAC-derived cell lines. Through transcriptomic analyses, we found that depletion of TRIP12 significantly downregulated the expression of genes targeted by the E2F transcription factors. It is known that E2F transcription family controls the expression of genes implicated in G₁-S and G₂/M transition [55]. Interestingly, our analysis further uncovered that TRIP12 depletion specifically affected the expression of E2F-target genes associated with cell division, suggesting that TRIP12 plays a crucial role in the appropriate expression of genes essential for this phase transition. This observation aligns with the finding that TRIP12 is necessary for cell division and chromosome segregation [41].

Moreover, our findings highlighted the key role of TRIP12 in acinar cell identity and plasticity by showing that a loss of TRIP12 prevented the reprogramming process in response to pancreatic inflammation. Of importance, TRIP12 deficiency also impedes the formation of ADM in the presence of *Kras*^{G12D}, which favors a role for TRIP12 in oncogenic transformation. We demonstrated that TRIP12 induces a poly-ubiquitination-dependent degradation of the transcription factor PTF1A, a maintenance keeper of acinar phenotype [43]. Therefore, it is possible that TRIP12 ablation in acinar cells stabilizes PTF1A expression, which could maintain an acinar phenotype even in the presence of inflammation or *Kras*^{G12D} expression. Moreover, during ADM, epigenetic repression of acinar enzymes and transcription factors is initiated and

Figure 4. TRIP12 is required for ADM formation *ex vivo* and *in vivo*. (A and B) Representative bright field images (top panels) and bright field + fluorescence images (bottom panels) of acinar cell clusters and ductal cyst structures from isolated acinar cells from control ZsG-C and ZsG-E and TRIP12-deficient ZsG-CT and ZsG-ET pancreas 1 and 4 days after isolation and treatment with EGF. Both *Trip12*^{+/+} and *Trip12*^{fl/fl} mice were bred with ZsGreen reporter mice prior to crossing with *Elas*-CreERT2 mice or *Pdx1*-Cre mice yielding ZsGreen expression in control ZsG-C and ZsG-E and in ZsG-CT and ZsG-ET TRIP12-deficient acinar cells: d, ductal cyst structures formed after ADM; ab, abnormal cell clusters with enlarged lumen or vacuoles. Images are representative of three independent experiments. (C and D) Quantification of fluorescent cellular structures: acinar cell clusters, ductal cyst structures, and abnormal cell clusters 4 days after acinar cell isolation from ZsG-E and ZsG-C control and ZsG-ET and ZsG-CT pancreas and treatment with EGF. The bars represent the mean ± SEM of three independent experiments. A Kruskal–Wallis test was used. (E) Experimental design of caerulein-induced acute pancreatitis in ET and E control mice. Inactivation of *Trip12* was induced by injections of tamoxifen at age 7 weeks. Controls were also treated with tamoxifen. Pancreatitis was induced 1 week later. Mice were sacrificed 2 h, 1 day, and 5 days after last injection. (F) Plasma amylase levels of E and ET mice were determined at 2 h, 1 day, or 5 days after the last injection of caerulein. Results were obtained from three independent experiments and expressed as mean ± SEM. A Mann–Whitney test was applied. (G) Representative H/E staining of E and ET mice (*n* = 3) pancreas 2 h, 1 day, and 5 days after the last injection of caerulein. Green arrowheads indicate control acinar cells with central distended lumen at 2 h that evolve toward a ductal phenotype 1 day after treatment (yellow asterisks). Yellow arrows indicate vacuoles of various sizes that sometimes contain amorphous material (green asterisks). Yellow hashes correspond to apoptotic cells. Gray arrows indicate inflammatory cells in interstitial edema. (H) Representative immunofluorescence images of cytokeratin 19 (CK19) expression at indicated times after last caerulein injection obtained from three experiments with three different mice. Nuclei were counterstained with DAPI. d, duct; yellow asterisks, transdifferentiating acini; yellow arrows, vacuoles.

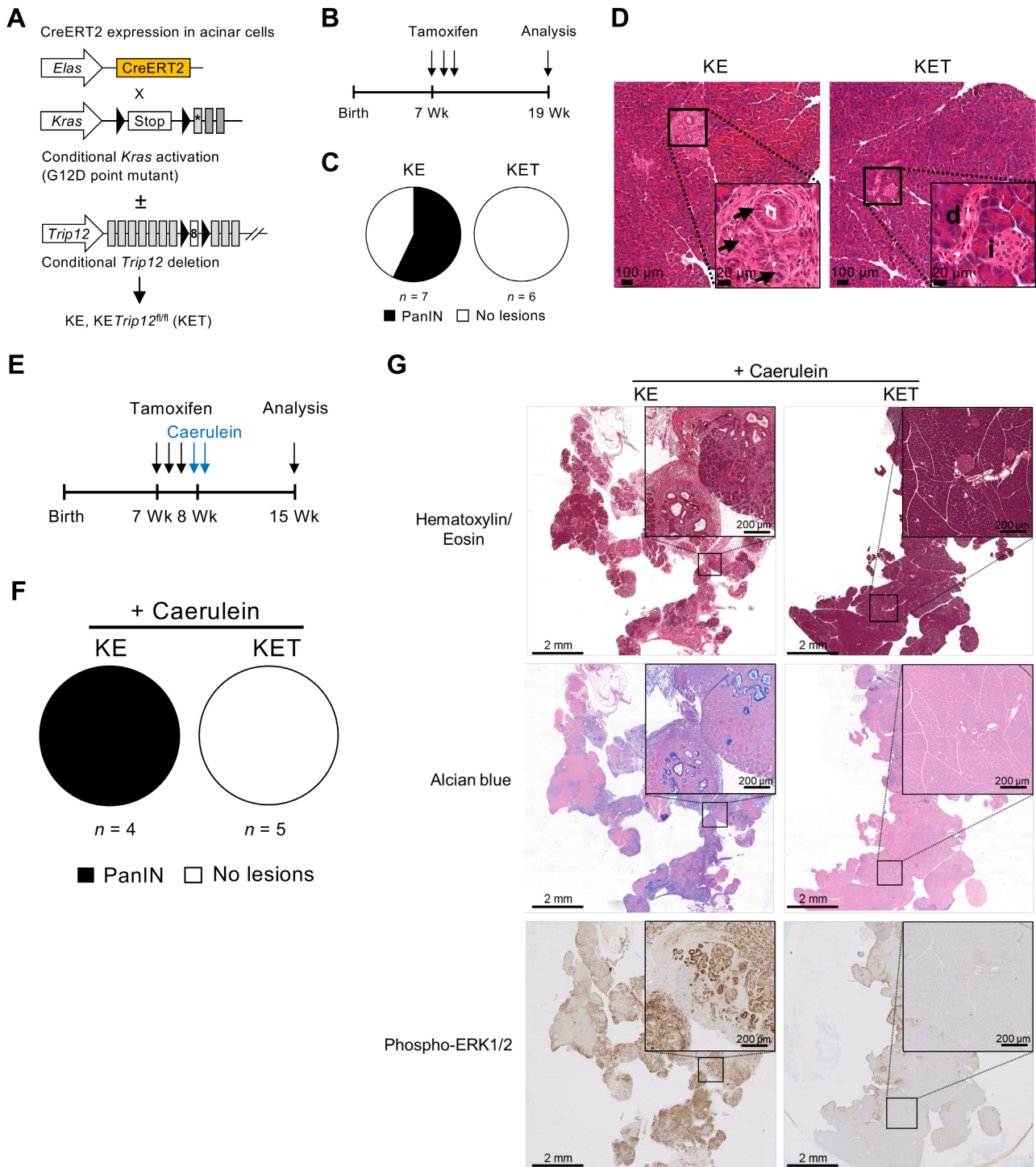


Figure 5. TRIP12 participates in PDAC initiation. (A) Schematic representation of KET mouse model. Black triangles indicate loxP sequences. (B) Experimental design of *Trip12* deletion and *Kras*^{G12D} activation induced by tamoxifen at 7 weeks. Mice were sacrificed and analyzed at 19 weeks. (C) Incidence of precancerous PanIN lesions in KE ($n = 7$) and KET mice ($n = 6$). (D) Representative H/E staining of KE and KET mice pancreas at 19 weeks. Boxes indicate enlarged regions in insets. Black arrows indicate PanIN lesions. d, duct; i, islet. (E) Experimental design of *Trip12* deletion and *Kras*^{G12D} activation induced by tamoxifen at 7 weeks and treated by caerulein at 8 weeks. Mice were sacrificed and analyzed at 15 weeks. (F) Incidence of precancerous PanIN lesions in KE ($n = 4$) and KET mice ($n = 5$) treated with caerulein. (G) Representative H/E, Alcian blue staining and phospho-ERK1/2 IHC images of KE and KET mice pancreas treated with caerulein. Boxes indicate enlarged regions.

maintained by repressive histone marks H2AK119Ub and H3K27me3 added by histone-modifying enzymes of the Polycomb repressive complexes (PRC) 1 and 2 [56,57]. TRIP12 is reported to interact with several components of PRC (e.g., EED, SUZ12, and ASXL1)

[58–60] or to control the stability of chromatin remodeling complexes such as switch/sucrose nonfermentable (SWI/SNF) [35,38]. Given these multiple roles on chromatin, it is likely that TRIP12 depletion in acinar cells perturbs the

regulation of transcription, which would lead to an inhibition of reprogramming processes required for ADM.

Finally, our research uncovered that while TRIP12 is essential for the initiation of cancer, it becomes dispensable for PDAC progression when the oncogenic mutation

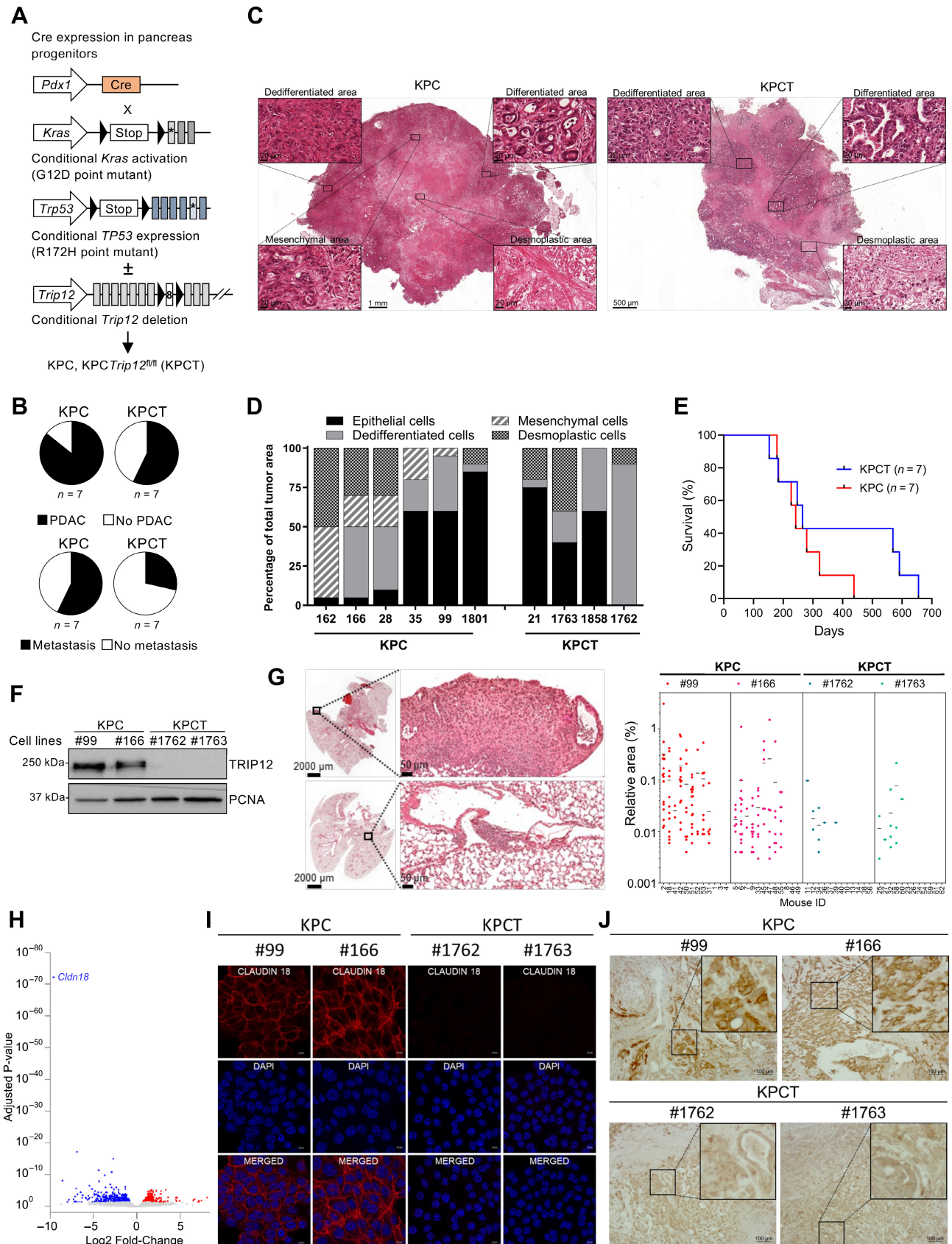


Figure 6 Legend on next page.

Kras^{G12D} is associated with the *TP53*^{R172H} oncogene. Interestingly, the survival curves of mice mirror those observed in human patients. While the median survival time is not impacted by the level of TRIP12 expression, both human patients with tumors expressing low levels of TRIP12 and TRIP12-knockout KPC mice exhibit, on average, longer lifespans. We also noticed that, whereas the absence of TRIP12 does not suppress tumorigenic potential in the presence of *Kras*^{G12D} and *Trp53*^{R172H}, TRIP12 participates in the invasive capacity of tumor cells and the presence of a mesenchymal component. Previous data from the literature reported that TRIP12 represses EMT and mesenchymal traits [61]. Our transcriptome analysis did not unveil significant impacts of TRIP12 depletion on EMT mRNA signatures. However, it demonstrated that TRIP12 was likely necessary for the expression of the tight junction protein CLAUDIN 18. Two *CLAUDIN18* transcripts are produced by an alternative splicing [62]. The silencing of the *CLAUDIN18.2* isoform in the vast majority of normal tissues has been related to its promoter hypermethylation [63,64] and transcriptional activation [63–65]. Moreover, in KC mice, the depletion of *Arid1a* gene expression (AT-rich interactive domain 1) that encodes a subunit of the SWI/SNF chromatin remodeling complex induces a dramatic expression of CLAUDIN 18 [66]. TRIP12 regulates the stability of the SWI/SNF remodeling complex by targeting the protein BAF57 [35,67]. It is therefore tempting to speculate that TRIP12 modulates CLAUDIN 18 expression via its action of the SWI/SNF complex. In pancreatic oncogenesis, *CLAUDIN 18.2* appears in precancerous lesions [53,68–70], and an increased expression correlates with the presence of distant metastasis [71]. In human PDAC, CLAUDIN 18 expression is associated with well-differentiated tumors and a better prognosis [53,72]. Therefore, the fact that a TRIP12 depletion reduces the metastatic dissemination of KPC tumors and the invasive capacity of KPC tumor-derived cells remains to be explained. However, the main function of the ubiquitin ligase TRIP12 is to provoke the degradation of target proteins. TRIP12 depletion likely induces the expression of other proteins, which leads to a reduced

invasion capacity of PDAC cancer cells regardless of CLAUDIN 18 expression.

In summary, the involvement of HECT E3 ubiquitin ligases in the initiation and progression of PDAC has been insufficiently explored until now. Our research has pinpointed TRIP12 as a crucial factor in acinar-to-ductal reprogramming, in the formation of *Kras*^{G12D}-driven PanINs and in tumor invasion. These findings could give rise to new strategies aimed at maintaining acinar differentiation. Therefore, the targeting of overexpressed TRIP12 would contribute to inhibiting *Kras*^{G12D}-driven tumorigenesis.

Acknowledgements

We thank F Fiore from Centre d'Immunophénomique (CIPHE) (Marseille, France) service monitoring, all members of the animal facility at CREFRE (UMS 006), Imag'IN platform and the Pathology Department of Institut Universitaire du Cancer de Toulouse and C. Segura from the histology platform of Institut des Maladies Métaboliques et Cardiovasculaires de Toulouse. We thank F. Larminat (Institut de Pharmacologie et de Biologie Structurale of Toulouse) and L. Bartholin (Centre de Recherche en Cancérologie de Lyon) for helpful discussions. We also thank the technological platforms of the Cancer Research Center of Toulouse (L. Ligat and L. Lestienne) and the GET-TRI platform (INRAE-Saint Martin du Touch). We thank S. Arcucci and N. Therville for technical help. This project was funded by the Ligue contre le cancer, the Fondation Toulouse Cancer-Santé (TCS2018CS079), the Association Française pour la Recherche sur le Cancer du Pancréas, and the Cancéropôle Grand Sud-Ouest (2021-EM22). MB was funded by the University Paul Sabatier (Toulouse) and the Ligue contre le cancer. CV was funded by the University Paul Sabatier (Toulouse) and the Ligue contre le cancer. DV was funded by the Ecole Normale Supérieure (Paris). DL was funded by the Ligue contre le Cancer. AR is funded by University Paul Sabatier (Toulouse).

Figure 6. TRIP12 participates in PDAC metastatic dissemination and CLAUDIN 18 expression. (A) Schematic representation of KPC and KPCT models. Black triangles indicate loxP sequences. (B) Incidence of PDAC and metastasis in KPC ($n = 7$) and KPCT ($n = 7$) mice. The number of mice with PDAC (top panel) and metastasis (bottom panel) is represented in black. (C) Representative H/E staining of KPC and KPCT tumors. Black boxes indicate enlarged regions of dedifferentiated, differentiated, mesenchymal, and desmoplastic areas. (D) Surface occupied by dedifferentiated, differentiated, mesenchymal, and desmoplastic cells in KPC ($n = 6$) and KPCT ($n = 4$) tumors expressed as percentage of total tumor area. Mouse IDs are indicated on x-axis. (E) Percentage of survival of KPC and KPCT mice. (F) TRIP12 protein expression in murine cell lines derived from indicated KPC and KPCT tumors was determined by western blot analysis. PCNA protein level was used as loading control. The image is representative of three independent experiments. (G) Representative H/E staining of lung metastases in mice obtained after indicated cell lines were injected via tail vein (left panel). Black boxes indicate enlarged regions. Relative area of metastases in mouse lungs after injection of indicated cell lines via tail vein ($n = 12$ per cell line) (right panel). The surface area of metastases was measured on two whole lung sections per mouse and normalized to the total lung area. Results are presented as relative area of all metastases for each mouse. Mouse IDs are indicated on x-axis. (H) Volcano plot of mRNA with differential expression in three KPCT cell lines compared to three KPC cell lines as determined using RNA-seq. Blue and red dots indicate mRNA with reduced or increased expression, respectively. Gray dots correspond to mRNA with a p value lower than 0.05. (I) Representative immunofluorescence images of CLAUDIN 18 expression in indicated KPC and KPCT cell lines. Nuclei were counterstained with DAPI. (J) Representative IHC staining of CLAUDIN 18 expression in indicated KPC and KPCT tumors. Black boxes indicate enlarged regions.

Author contributions statement

Animal studies were performed by MB under the supervision of MD with the assistance of CV and HL. *Ex vivo* experiments were performed by MB, CV and MF. Immunohistochemical and microscopic analyses were performed by MD, LP, JT and FC and quantified by MB, MD, JT, AC and JS. Computational analyses were performed by DV, MD and JT. Cellular biology and genomic analyses were performed by MB, JT, DL, DV, AR, NH and GL. VG, PC and JG-G participated in the design of the study and in the critical review of the manuscript. The experiments were designed by MD and JT, who wrote the manuscript, which was approved by all the authors.

Data availability statement

Agilent microarray gene expression data are publicly available in the Gene Expression Omnibus (GEO) repository (GSE147717 and GSE147549): <https://www.ncbi.nlm.nih.gov/geo/query/acc.cgi?acc=GSE147717>; <https://www.ncbi.nlm.nih.gov/geo/query/acc.cgi?acc=GSE147549> RNA-seq data are publicly available in the GEO repository (GSE221587): <https://www.ncbi.nlm.nih.gov/geo/query/acc.cgi?acc=GSE221587>.

References

- Siegel DA, King JB, Lupo PJ, *et al.* Counts, incidence rates, and trends of pediatric cancer in the United States, 2003–2019. *J Natl Cancer Inst* 2023; **115**: 1337–1354.
- Sahin IH, Lowery MA, Stadler ZK, *et al.* Genomic instability in pancreatic adenocarcinoma: a new step towards precision medicine and novel therapeutic approaches. *Expert Rev Gastroenterol Hepatol* 2016; **10**: 893–905.
- Neuzillet C, Gaujoux S, Williet N, *et al.* Pancreatic cancer: French clinical practice guidelines for diagnosis, treatment and follow-up (SNFGE, FFCD, GERCOR, UNICANCER, SFCD, SFED, SFRO, ACHBT, AFC). *Dig Liver Dis* 2018; **50**: 1257–1271.
- Bockman DE, Guo J, Büchler P, *et al.* Origin and development of the precursor lesions in experimental pancreatic cancer in rats. *Lab Invest* 2003; **83**: 853–859.
- Pinho AV, Rooman I, Reichert M, *et al.* Adult pancreatic acinar cells dedifferentiate to an embryonic progenitor phenotype with concomitant activation of a senescence programme that is present in chronic pancreatitis. *Gut* 2011; **60**: 958–966.
- Strobel O, Dor Y, Alsina J, *et al.* In vivo lineage tracing defines the role of acinar-to-ductal transdifferentiation in inflammatory ductal metaplasia. *Gastroenterology* 2007; **133**: 1999–2009.
- Kong B, Bruns P, Behler NA, *et al.* Dynamic landscape of pancreatic carcinogenesis reveals early molecular networks of malignancy. *Gut* 2018; **67**: 146–156.
- Clerc P, Leung-Theung-Long S, Wang TC, *et al.* Expression of CCK2 receptors in the murine pancreas: proliferation, transdifferentiation of acinar cells, and neoplasia. *Gastroenterology* 2002; **122**: 428–437.
- Gidekel Friedlander SY, Chu GC, Snyder EL, *et al.* Context-dependent transformation of adult pancreatic cells by oncogenic K-Ras. *Cancer Cell* 2009; **16**: 379–389.
- Habbe N, Shi G, Meguid RA, *et al.* Spontaneous induction of murine pancreatic intraepithelial neoplasia (mPanIN) by acinar cell targeting of oncogenic Kras in adult mice. *Proc Natl Acad Sci U S A* 2008; **105**: 18913–18918.
- Prévot P-P, Simion A, Grimont A, *et al.* Role of the ductal transcription factors HNF6 and Sox9 in pancreatic acinar-to-ductal metaplasia. *Gut* 2012; **61**: 1723–1732.
- Ferreira RMM, Sancho R, Messal HA, *et al.* Duct- and acinar-derived pancreatic ductal adenocarcinomas show distinct tumor progression and marker expression. *Cell Rep* 2017; **21**: 966–978.
- Quilichini E, Fabre M, Dirami T, *et al.* Pancreatic ductal deletion of Hnf1b disrupts exocrine homeostasis, leads to pancreatitis, and facilitates tumorigenesis. *Cell Mol Gastroenterol Hepatol* 2019; **8**: 487–511.
- Lee AYL, Dubois CL, Sarai K, *et al.* Cell of origin affects tumour development and phenotype in pancreatic ductal adenocarcinoma. *Gut* 2019; **68**: 487–498.
- Arias AE, Bendayan M. Differentiation of pancreatic acinar cells into duct-like cells in vitro. *Lab Invest* 1993; **69**: 518–530.
- Rooman I, Real FX. Pancreatic ductal adenocarcinoma and acinar cells: a matter of differentiation and development? *Gut* 2012; **61**: 449–458.
- Vila MR, Lloreta J, Real FX. Normal human pancreas cultures display functional ductal characteristics. *Lab Invest* 1994; **71**: 423–431.
- Fanjul M, Gmyr V, Sengenès C, *et al.* Evidence for epithelial-mesenchymal transition in adult human pancreatic exocrine cells. *J Histochem Cytochem* 2010; **58**: 807–823.
- Shibata H, Komura S, Yamada Y, *et al.* In vivo reprogramming drives Kras-induced cancer development. *Nat Commun* 2018; **9**: 2081.
- Assi M, Achouri Y, Loriot A, *et al.* Dynamic regulation of expression of KRAS and its effectors determines the ability to initiate tumorigenesis in pancreatic acinar cells. *Cancer Res* 2021; **81**: 2679–2689.
- Guerra C, Collado M, Navas C, *et al.* Pancreatitis-induced inflammation contributes to pancreatic cancer by inhibiting oncogene-induced senescence. *Cancer Cell* 2011; **19**: 728–739.
- Guerra C, Schuhmacher AJ, Cañamero M, *et al.* Chronic pancreatitis is essential for induction of pancreatic ductal adenocarcinoma by K-Ras oncogenes in adult mice. *Cancer Cell* 2007; **11**: 291–302.
- Del Poggetto E, Ho I-L, Balestrieri C, *et al.* Epithelial memory of inflammation limits tissue damage while promoting pancreatic tumorigenesis. *Science* 2021; **373**: eabj0486.
- Hoang CQ, Hale MA, Azevedo-Pouly AC, *et al.* Transcriptional maintenance of pancreatic acinar identity, differentiation, and homeostasis by PTF1A. *Mol Cell Biol* 2016; **36**: 3033–3047.
- Kawaguchi Y, Cooper B, Gannon M, *et al.* The role of the transcriptional regulator Ptf1a in converting intestinal to pancreatic progenitors. *Nat Genet* 2002; **32**: 128–134.
- Krah NM, De La OJ-P, Swift GH, *et al.* The acinar differentiation determinant PTF1A inhibits initiation of pancreatic ductal adenocarcinoma. *Elife* 2015; **4**: e07125.
- Krah NM, Narayanan SM, Yugawa DE, *et al.* Prevention and reversal of pancreatic tumorigenesis through a differentiation-based mechanism. *Dev Cell* 2019; **50**: 744–754.e4.
- Jakubison BL, Schweickert PG, Moser SE, *et al.* Induced PTF1a expression in pancreatic ductal adenocarcinoma cells activates acinar gene networks, reduces tumorigenic properties, and sensitizes cells to gemcitabine treatment. *Mol Oncol* 2018; **12**: 1104–1124.
- Kopp JL, von Figura G, Mayes E, *et al.* Identification of Sox9-dependent acinar-to-ductal reprogramming as the principal mechanism for initiation of pancreatic ductal adenocarcinoma. *Cancer Cell* 2012; **22**: 737–750.
- Morris JP 4th, Cano DA, Sekine S, *et al.* Beta-catenin blocks Kras-dependent reprogramming of acini into pancreatic cancer precursor lesions in mice. *J Clin Invest* 2010; **120**: 508–520.
- Shi G, DiRenzo D, Qu C, *et al.* Maintenance of acinar cell organization is critical to preventing Kras-induced acinar-ductal metaplasia. *Oncogene* 2013; **32**: 1950–1958.

32. Chen D, Shan J, Zhu W-G, et al. Transcription-independent ARF regulation in oncogenic stress-mediated p53 responses. *Nature* 2010; **464**: 624–627.
33. Chen D, Kon N, Zhong J, et al. Differential effects on ARF stability by normal versus oncogenic levels of c-Myc expression. *Mol Cell* 2013; **51**: 46–56.
34. An C-I, Ganio E, Hagiwara N. Trip12, a HECT domain E3 ubiquitin ligase, targets Sox6 for proteasomal degradation and affects fiber type-specific gene expression in muscle cells. *Skelet Muscle* 2013; **3**: 11.
35. Keppler BR, Archer TK. Ubiquitin-dependent and ubiquitin-independent control of subunit stoichiometry in the SWI/SNF complex. *J Biol Chem* 2010; **285**: 35665–35674.
36. Gudjonsson T, Altmeyer M, Savic V, et al. TRIP12 and UBR5 suppress spreading of chromatin ubiquitylation at damaged chromosomes. *Cell* 2012; **150**: 697–709.
37. Gatti M, Imhof R, Huang Q, et al. The ubiquitin ligase TRIP12 limits PARP1 trapping and constrains PARP inhibitor efficiency. *Cell Rep* 2020; **32**: 107985.
38. Brunet M, Vargas C, Larrieu D, et al. E3 ubiquitin ligase TRIP12: regulation, structure, and physiopathological functions. *Int J Mol Sci* 2020; **21**: 8515.
39. Cai J-B, Shi G-M, Dong Z-R, et al. Ubiquitin-specific protease 7 accelerates p14(ARF) degradation by deubiquitinating thyroid hormone receptor-interacting protein 12 and promotes hepatocellular carcinoma progression. *Hepatology* 2015; **61**: 1603–1614.
40. Wang L, Zhang P, Molkenkint DP, et al. TRIP12 as a mediator of human papillomavirus/p16-related radiation enhancement effects. *Oncogene* 2017; **36**: 820–828.
41. Larrieu D, Brunet M, Vargas C, et al. The E3 ubiquitin ligase TRIP12 participates in cell cycle progression and chromosome stability. *Sci Rep* 2020; **10**: 789.
42. Khan OM, Almagro J, Nelson JK, et al. Proteasomal degradation of the tumour suppressor FBW7 requires branched ubiquitylation by TRIP12. *Nat Commun* 2021; **12**: 2043.
43. Hanoun N, Fritsch S, Gayet O, et al. The E3 ubiquitin ligase thyroid hormone receptor-interacting protein 12 targets pancreas transcription factor 1a for proteasomal degradation. *J Biol Chem* 2014; **289**: 35593–35604.
44. Desai BM, Oliver-Krasinski J, De Leon DD, et al. Preexisting pancreatic acinar cells contribute to acinar cell, but not islet beta cell, regeneration. *J Clin Invest* 2007; **117**: 971–977.
45. Delpu Y, Lulka H, Sicard F, et al. The rescue of miR-148a expression in pancreatic cancer: an inappropriate therapeutic tool. *PLoS One* 2013; **8**: e55513.
46. Bankhead P, Loughrey MB, Fernández JA, et al. QuPath: open source software for digital pathology image analysis. *Sci Rep* 2017; **7**: 16878.
47. Chang J-W, Zhang W, Yeh H-S, et al. mRNA 3'-UTR shortening is a molecular signature of mTORC1 activation. *Nat Commun* 2015; **6**: 7218.
48. Kent LN, Leone G. The broken cycle: E2F dysfunction in cancer. *Nat Rev Cancer* 2019; **19**: 326–338.
49. Madisen L, Zwingman TA, Sunkin SM, et al. A robust and high-throughput Cre reporting and characterization system for the whole mouse brain. *Nat Neurosci* 2010; **13**: 133–140.
50. Grimont A, Leach SD, Chandwani R. Uncertain beginnings: acinar and ductal cell plasticity in the development of pancreatic cancer. *Cell Mol Gastroenterol Hepatol* 2022; **13**: 369–382.
51. Hingorani SR, Wang L, Multani AS, et al. Trp53R172H and KrasG12D cooperate to promote chromosomal instability and widely metastatic pancreatic ductal adenocarcinoma in mice. *Cancer Cell* 2005; **7**: 469–483.
52. Lücke J, Zhang T, Zazara DE, et al. Protocol for generating lung and liver metastasis in mice using models that bypass intravasation. *STAR Protoc* 2024; **5**: 102696.
53. Tanaka M, Shibahara J, Fukushima N, et al. Claudin-18 is an early-stage marker of pancreatic carcinogenesis. *J Histochem Cytochem* 2011; **59**: 942–952.
54. Wang C, Wu N, Pei B, et al. Claudin and pancreatic cancer. *Front Oncol* 2023; **13**: 1136227.
55. Bracken AP, Ciro M, Cocito A, et al. E2F target genes: unraveling the biology. *Trends Biochem Sci* 2004; **29**: 409–417.
56. Benitz S, Regel I, Reinhard T, et al. Polycomb repressor complex 1 promotes gene silencing through H2AK119 mono-ubiquitination in acinar-to-ductal metaplasia and pancreatic cancer cells. *Oncotarget* 2016; **7**: 11424–11433.
57. Benitz S, Straub T, Mahajan UM, et al. Ring1b-dependent epigenetic remodelling is an essential prerequisite for pancreatic carcinogenesis. *Gut* 2019; **68**: 2007–2018.
58. Kweon S-M, Chen Y, Moon E, et al. An adversarial DNA N⁶-methyladenine-sensor network preserves polycomb silencing. *Mol Cell* 2019; **74**: 1138–1147.e6.
59. Cao Q, Wang X, Zhao M, et al. The central role of EED in the orchestration of polycomb group complexes. *Nat Commun* 2014; **5**: 3127.
60. Oliviero G, Brien GL, Waston A, et al. Dynamic protein interactions of the polycomb repressive complex 2 during differentiation of pluripotent cells. *Mol Cell Proteomics* 2016; **15**: 3450–3460.
61. Lee KK, Rajagopalan D, Bhatia SS, et al. The oncogenic E3 ligase TRIP12 suppresses epithelial-mesenchymal transition (EMT) and mesenchymal traits through ZEB1/2. *Cell Death Discov* 2021; **7**: 95.
62. Niimi T, Nagashima K, Ward JM, et al. Claudin-18, a novel downstream target gene for the T/EBP/NKX2.1 homeodomain transcription factor, encodes lung- and stomach-specific isoforms through alternative splicing. *Mol Cell Biol* 2001; **21**: 7380–7390.
63. Sahin U, Koslowski M, Dhaene K, et al. Claudin-18 splice variant 2 is a pan-cancer target suitable for therapeutic antibody development. *Clin Cancer Res* 2008; **14**: 7624–7634.
64. Ito T, Kojima T, Yamaguchi H, et al. Transcriptional regulation of claudin-18 via specific protein kinase C signaling pathways and modification of DNA methylation in human pancreatic cancer cells. *J Cell Biochem* 2011; **112**: 1761–1772.
65. Yano K, Imaeda T, Niimi T. Transcriptional activation of the human claudin-18 gene promoter through two AP-1 motifs in PMA-stimulated MKN45 gastric cancer cells. *Am J Physiol Gastrointest Liver Physiol* 2008; **294**: G336–G343.
66. Ferri-Borgogno S, Barui S, McGee AM, et al. Paradoxical role of AT-rich interactive domain 1A in restraining pancreatic carcinogenesis. *Cancers (Basel)* 2020; **12**: 2695.
67. Kajiro M, Tsuchiya M, Kawabe Y-I, et al. The E3 ubiquitin ligase activity of Trip12 is essential for mouse embryogenesis. *PLoS One* 2011; **6**: e25871.
68. Karanjawala ZE, Illei PB, Ashfaq R, et al. New markers of pancreatic cancer identified through differential gene expression analyses: claudin 18 and annexin A8. *Am J Surg Pathol* 2008; **32**: 188–196.
69. Westmoreland JJ, Drosos Y, Kelly J, et al. Dynamic distribution of claudin proteins in pancreatic epithelia undergoing morphogenesis or neoplastic transformation. *Dev Dyn* 2012; **241**: 583–594.
70. Lee JH, Kim KS, Kim T-J, et al. Immunohistochemical analysis of claudin expression in pancreatic cystic tumors. *Oncol Rep* 2011; **25**: 971–978.
71. Wang X, Zhang C-S, Dong X-Y, et al. Claudin 18.2 is a potential therapeutic target for zolbetuximab in pancreatic ductal adenocarcinoma. *World J Gastrointest Oncol* 2022; **14**: 1252–1264.
72. Zhang Z, Liu X, Zhou L, et al. Investigation of clinical application of claudin 18 isoform 2 in pancreatic ductal adenocarcinoma: a

- retrospective analysis of 302 chinese patients. *Histol Histopathol* 2022; **37**: 1031–1040.
73. Tang Z, Li C, Kang B, *et al.* GEPIA: a web server for cancer and normal gene expression profiling and interactive analyses. *Nucleic Acids Res* 2017; **45**: W98–W102.
74. Seo BA, Kim D, Hwang H, *et al.* TRIP12 ubiquitination of glucocerebrosidase contributes to neurodegeneration in Parkinson's disease. *Neuron* 2021; **109**: 3758–3774.e11.
- References 73 and 74 are cited only in the supplementary material.

SUPPLEMENTARY MATERIAL ONLINE

Supplementary materials and methods

Figure S1. Percentage of TRIP12-positive cells in human PDAC-derived cell lines

Figure S2. Genomic and DNA methylation analyses of *TRIP12* gene in human PDAC-derived cell lines

Figure S3. Short and long forms of *TRIP12* mRNA in human PDAC-derived cell lines

Figure S4. TRIP12 protein cellular localization during the cell cycle of human PDAC-derived cell lines

Figure S5. *TRIP12* mRNA level, TRIP12 protein level, and survival assay of PANC-1 and MIA PaCa-2 cells expressing shRNAs directed against *TRIP12* mRNA

Figure S6. Weight and volume of ShTRIP12 GLuc MIA PaCa-2 tumors. Adherence capacity of TRIP12 depleted-PANC-1 and MIA PaCa-2 cells

Figure S7. Gene set enrichments of TRIP12 depleted-PANC-1 and MIA PaCa-2 cells

Figure S8. Physical interaction networks of proteins encoded by E2 target gene set and TRIP12-depleted MIA PaCa-2 E2F target leading edge genes

Figure S9. Immunofluorescence images of TRIP12 in C mice pancreas and transcriptomic analysis of TRIP12-depleted acinar preparation

Figure S10. Morphological analysis of ET mouse model

Figure S11. ZsGreen expression in ZsG-CT and ZsG-ET mouse models

Figure S12. Quantification of pancreatic injury in E and ET pancreas

Figure S13. Pancreas/body weight ratio, pancreas weight, and mouse weight of KE and KET mice

Figure S14. Morphological analyses of KPC and KPCT tumors. Invasive capacity and CLAUDIN 18 expression of KPC- and KPCT-derived cell lines

Table S1. List of antibodies used

Table S2. Primer sequences

Table S3. Clinical features of PDAC patients and tumors

Table S4. GSEA